Bachelor Thesis

Searching for Mg II absorption in quasar spectra near E+A post-starburst galaxies with fast outflows

Harsh Sureshbhai Satasiya

Master student in Physics

Faculty of Physics and Astronomy
Ruhr-Universität Bochum

Supervisor: Prof. Dr. Dominik Bomans
Submitted: April 2025

Acknowledgements

I would like to express my sincere gratitude to my supervisor, Prof. Dr. Dominik Bomans, for his guidance, support, and encouragement throughout this project. His insights and feedback were invaluable in shaping the direction of this thesis.

Special thanks go to the developers and maintainers of the SDSS and NED databases, as well as the teams behind the `Astropy`, `Specutils`, and `Astroquery` Python libraries, which played a central role in enabling the analysis performed in this work.

I would also like to thank OpenAI's ChatGPT for assisting in debugging Python code throughout the course of this thesis. Its support was particularly valuable in troubleshooting technical challenges.

Finally, I would like to thank my family and friends for their patience, encouragement, and moral support throughout the time I was working on this thesis.

Abstract

This thesis explores the presence of Mg II absorption in the spectra of background quasars located near post-starburst (E+A) galaxies, with the aim of tracing possible large-scale outflows or circumgalactic medium (CGM) structures. A sample of post-starburst galaxies was selected from the Sloan Digital Sky Survey (SDSS), and nearby quasars within a projected radius of 10 arcminutes were identified using cross-matching with the NASA/IPAC Extragalactic Database (NED). For each system, Mg II $\lambda\lambda$2796, 2803 Å absorption features were examined in both the galaxy and quasar spectra.

The galaxy spectra consistently exhibited blueshifted Mg II absorption with velocity offsets typically ranging from several hundred to over 1000 $\mathrm{km\,s^{-1}}$, consistent with feedback-driven outflows. However, in the majority of quasar spectra, no corresponding Mg II absorption was detected at the expected positions based on the galaxy redshifts. In a few cases, redshifted or ambiguous features were observed, but these did not match the expected signature of galactic outflows.

The results suggest that while outflows are clearly visible in the galaxy spectra, they do not commonly manifest along nearby lines of sight probed by background quasars, at least within the scale and sensitivity limits of this dataset. These findings imply that the absorbing material may be confined to small spatial scales or exhibit anisotropic distribution.

Contents

List of Figures

List of Tables

1 Introduction

Understanding how galaxies evolve over time is a central challenge in astrophysics. Among the various transitional phases, post-starburst galaxies—also known as E+A galaxies—represent a brief but critical stage. These galaxies are characterized by strong Balmer absorption lines from A-type stars, indicating a recent burst of star formation, but show little to no ongoing star formation activity. The sharp transition suggests that star formation was rapidly quenched, making these galaxies ideal laboratories for studying galaxy evolution and feedback mechanisms.

One proposed mechanism for this sudden quenching involves powerful galactic outflows. These outflows can eject cold gas from the galaxy, preventing future star formation. The presence and velocity of such outflows can be inferred from blueshifted absorption lines in the galaxy's spectrum, especially from metal lines like Mg II (2796, 2803 Å). These lines are sensitive tracers of cool, enriched gas and are frequently used to study galactic winds.

A complementary approach to studying galactic environments involves using quasars as background light sources. When a quasar is located near a galaxy on the sky, its light can pass through the galaxy's interstellar medium (ISM) or circumgalactic medium (CGM), imprinting absorption features onto the quasar's spectrum. By analyzing these absorption lines, we gain insight into the material surrounding or in front of the galaxy, including potential outflows.

The central goal of this thesis is to explore whether the observed Mg II absorption in quasar spectra near E+A post-starburst galaxies originates from the galaxies' own outflows or from intervening material along the line of sight. To do this, we compare the absorption features in galaxy spectra with those in the spectra of nearby quasars, analyzing their velocity shifts and redshifts to assess consistency and potential physical connections.

This thesis is structured as follows: Chapter 2 introduces the theoretical background related to post-starburst galaxies, galactic outflows, and absorption line diagnostics. Chapter 3 details the data selection and methodology used to extract and analyze spectra. Chapter 4 presents the results of the spectral analysis. Chapter 5 discusses the implications of the findings, and Chapter 6 concludes with a summary and outlook.

2 Theory

2.1 Post-Starburst Galaxies

Post-starburst galaxies, often referred to as E+A or K+A galaxies, are a rare and intriguing class of galaxies that represent a transitional phase in the evolutionary sequence of galaxies. They are characterized by spectral features that simultaneously show evidence of a recent, intense starburst and a sudden cessation of star formation. This is indicated by strong Balmer absorption lines, particularly from A-type stars, which dominate the light of the galaxy, coupled with a notable lack of nebular emission lines such as [O II] and H α, which are typical indicators of ongoing star formation [19].

The classification "E+A" stems from their spectral appearance, which resembles a combination of elliptical galaxy (E) features and A-type star absorption lines. These galaxies do not show the signatures of active star-forming regions, making them stand out in spectral surveys. The lack of emission lines, alongside strong absorption from young stars, suggests that these galaxies have experienced a recent starburst event that was abruptly quenched [19].

2.1.1 Formation Mechanisms

Post-starburst galaxies are often thought to form as a result of major galaxy mergers or interactions. Such interactions can funnel large amounts of cold gas into the central regions of a galaxy, igniting a burst of star formation. This process consumes or redistributes much of the available gas. The subsequent quenching of star formation may be triggered by feedback mechanisms such as active galactic nuclei (AGN) activity, which heats or expels the remaining gas, or by supernova-driven winds that remove or disrupt the gas reservoir [7].

Simulations and observations suggest that mergers not only trigger starbursts but also drive the structural transformation of galaxies. Tidal features, such as tails or shells, are frequently observed in post-starburst galaxies, supporting the idea of recent dynamical disturbances. These structural signatures often fade over time, which is why they are more commonly seen in younger post-starburst systems [7].

2.1.2 Gas Content and Quenching Puzzles

Contrary to the earlier assumption that post-starburst galaxies are gas-poor following the quenching event, recent observations have revealed that many of these galaxies retain substantial reservoirs of molecular gas. Data from the Atacama Large Millime-

ter/submillimeter Array (ALMA) and other observatories show that this gas is often concentrated near the centers of galaxies, suggesting it was not expelled entirely. Despite the presence of this fuel for star formation, new star formation is largely absent [13].

This paradox raises important questions about what physical mechanisms suppress star formation in post-starburst galaxies. Some hypotheses include increased turbulence, shocks, or heating of the gas, all of which may inhibit the collapse of gas clouds into stars. Understanding why these galaxies retain gas but fail to reignite star formation is crucial to unraveling the processes governing galaxy evolution [13].

2.1.3 Visual Representations

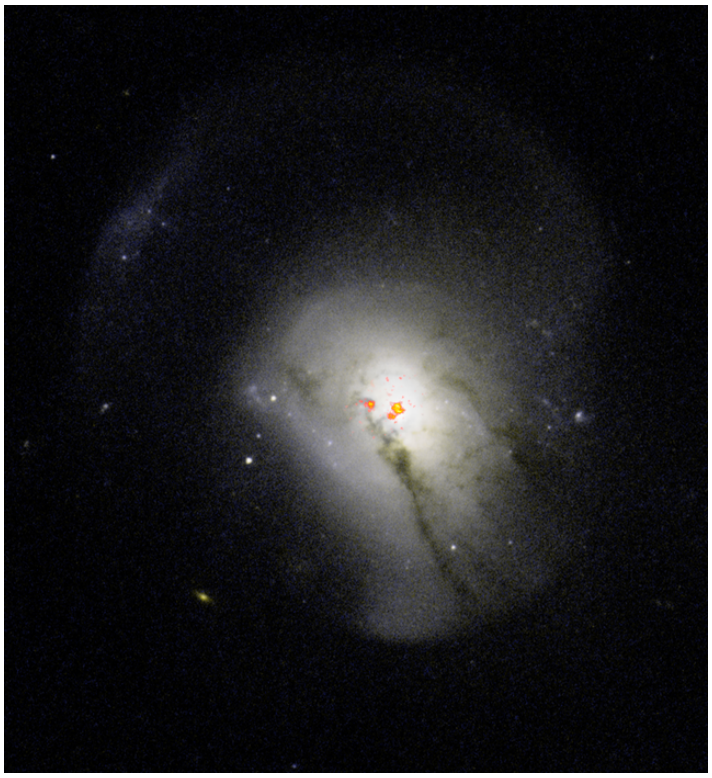

Figure 1: Hubble image of a post-starburst galaxy showing dense gas near the center and signs of past interaction. Source: [8].

Including visual data can further illustrate the complex morphology of post-starburst galaxies. High-resolution images, such as those from the Hubble Space Telescope, often reveal signs of recent mergers, including irregular morphologies, tidal features, and compact cores. One example is the post-starburst galaxy SDSS J0912+1523, which has been studied in depth for its compact, gas-rich central region and lack of star formation [8].

These visual representations not only support the theoretical understanding of their formation and evolution but also help confirm the presence of structural features predicted by simulations.

Post-starburst galaxies are key to understanding the rapid quenching processes that shape the galaxy population in the universe. They offer a window into the physical conditions that can halt star formation quickly and help explain how galaxies transition from active star-forming states to more passive evolutionary phases.

2.2 Mg II and Other Spectral Lines

Spectral lines serve as vital tools in astrophysics, providing insights into the physical and chemical properties of celestial objects. Among these, the Mg II doublet and lines such as [O II] and Fe II are particularly significant in studying the interstellar and circumgalactic media.

2.2.1 Mg II Doublet (2796, 2803 Å): Resonance Lines Sensitive to Cool Gas

The Mg II resonance doublet, consisting of lines at 2796 Å and 2803 Å, is a powerful tracer of cold gas at temperatures around 10^4 K. Due to its resonance nature and ionization potential similar to that of neutral hydrogen, Mg II emission can trace cold gas properties through scattering processes akin to Lyman-alpha. Studies have shown that the Mg II doublet is effective in probing the distribution and kinematics of cold gas in and around galaxies [2].

2.2.2 [O II] (3726, 3729 Å) and Fe II: Diagnostic Power for Outflows and the Circumgalactic Medium

The [O II] doublet at 3726 Å and 3729 Å is commonly used to estimate star formation rates in galaxies. These lines can also reveal ionized outflows, as demonstrated by observations of massive compact galaxies exhibiting extended [O II] emission indicative of large-scale galactic winds [16].

Fe II absorption lines are valuable diagnostics for studying the multiphase nature of galactic outflows. The presence of Fe II* emission, often accompanying Mg II features, can indicate resonant scattering in an expanding wind, providing insights into the physical conditions and kinematics of the outflowing gas [15].

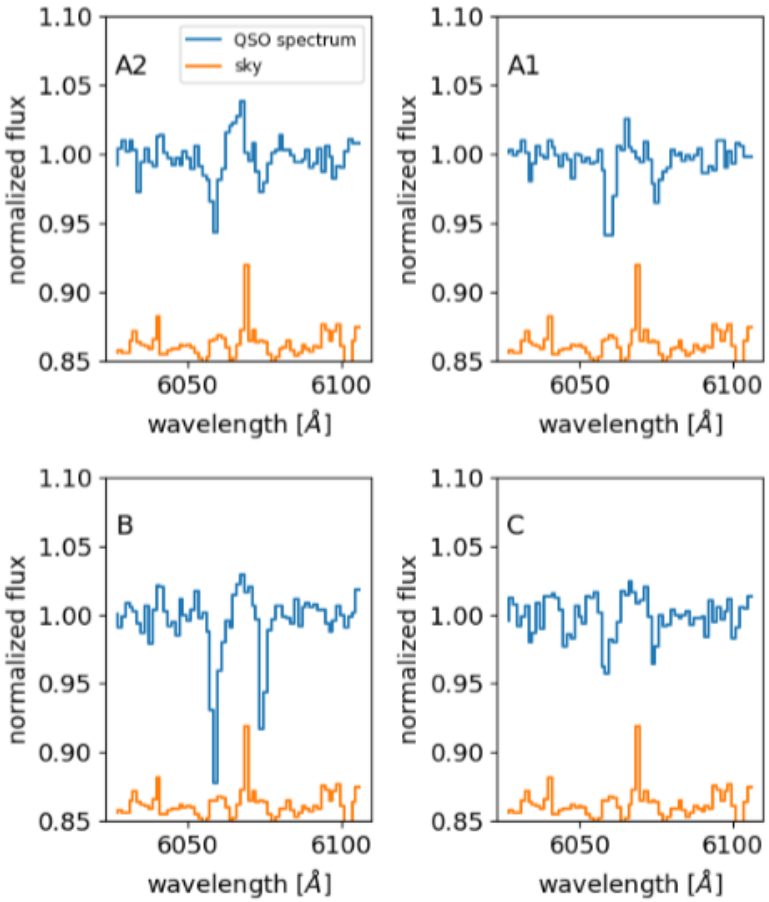

Figure 2: Mg II absorption features observed in quasar spectra at $z_{\text{abs}} = 1.168$. Both lines of the Mg II doublet are clearly detected in all four spectra. The offset orange lines represent the sky spectrum.

[3]

2.2.3 Interpreting Line Shifts: Insights into Kinematics

Shifts in spectral lines, such as the Mg II doublet, provide crucial information about the kinematics of gas in galaxies. For instance, the Mg II doublet ratio can vary with outflow or inflow velocities, with significant deviations observed at velocities exceeding 700 km/s. A doublet ratio $R_{\text{MgII}} < 1$ serves as an unambiguous tracer for powerful galactic winds, offering insights into the dynamics of gas flows within and around galaxies [2].

Understanding these spectral lines and their shifts is essential for probing the physical conditions, chemical compositions, and dynamic processes occurring in galaxies, contributing significantly to our knowledge of galaxy formation and evolution.

2.3 Galactic Outflows

Galactic outflows are large-scale gaseous ejections from galaxies, capable of carrying substantial amounts of material into the circumgalactic or even intergalactic medium. In the context of post-starburst galaxies, these outflows are especially significant, as they are believed to contribute to the abrupt quenching of star formation that defines this galaxy class.

2.3.1 Outflows in Post-Starburst Galaxies

Post-starburst galaxies frequently exhibit multiphase outflows, including ionized, atomic, and molecular gas. These outflows can persist for hundreds of millions of years after the starburst event, playing a crucial role in maintaining the quiescent nature of these systems. Studies have found that such winds are prevalent in compact post-starburst systems, where the compact morphology and high surface density may aid in sustaining outflows [20].

Figure 3: Hubble Space Telescope image of the starburst galaxy M82, also known as the Cigar Galaxy. This galaxy exhibits powerful galactic outflows, visible as red filaments extending from its central region. These outflows are driven by intense star formation and stellar feedback.

[12]

2.3.2 Driving Mechanisms: AGN and Stellar Feedback

The primary mechanisms thought to drive these galactic outflows are stellar feedback—mainly from supernovae following a burst of star formation—and active galactic nuclei (AGN). AGN feedback, in particular, is capable of expelling massive amounts of gas from galaxy centers at high velocities, thereby halting star formation. Observational evidence points to AGN-driven outflows as a key quenching mechanism in post-starburst systems [4].

2.3.3 Effects on Galaxy Evolution

These outflows not only remove the cold gas reservoir needed for star formation but also heat or ionize the remaining gas, further suppressing star formation activity. Additionally, expelled gas enriches the circumgalactic medium (CGM) with metals and dust, influencing future galaxy formation processes in the surrounding environment. This feedback loop is essential in transforming galaxies from blue, star-forming systems into red, quiescent ones [11].

2.4 Quasar Absorption Spectroscopy

Quasar absorption spectroscopy is a powerful method to investigate the properties of gas in the interstellar medium (ISM), the circumgalactic medium (CGM), and the intergalactic medium (IGM). By observing the spectra of distant quasars—bright active galactic nuclei with strong, continuous emission—astronomers can detect absorption features imprinted by gas clouds that lie along the line of sight.

2.4.1 Principle of the Technique

As light from a background quasar travels through the universe, it encounters gas associated with intervening galaxies or diffuse structures. Elements in this gas absorb photons at specific wavelengths, producing narrow absorption lines. By identifying these lines and measuring their redshifts, one can infer the presence, composition, and kinematics of the absorbing material [18].

This method is especially useful for probing low-density environments where emission may be too faint to detect. It has become essential in studying the CGM and IGM, providing insights into how galaxies exchange matter with their surroundings.

2.4.2 Application to Post-Starburst Galaxies

In this thesis, quasars are used as backlights to examine whether the absorption seen near post-starburst galaxies is intrinsic—arising from the galaxy's own outflows—or due to intervening material along the line of sight. The Mg II doublet is particularly valuable in this context, as it traces cool gas potentially ejected in galactic winds [10].

Comparing the Mg II absorption profiles in both galaxy and nearby quasar spectra allows one to distinguish between outflow signatures and absorption from unrelated foreground structures. This differential approach helps isolate the physical processes active in post-starburst environments.

2.4.3 Intrinsic vs. Intervening Absorption

A critical aspect of analysis is distinguishing between intrinsic absorption (from the host galaxy or its immediate CGM) and intervening absorption (from unrelated structures along the light path). This distinction is made based on the alignment of absorption redshifts with the systemic redshift of the galaxy, the velocity spread of the lines, and the presence of associated emission features [6].

When absorption is blueshifted relative to the galaxy redshift and found in both the galaxy spectrum and a nearby quasar's sightline, it can imply a coherent outflow or halo structure. Conversely, mismatched features may indicate unrelated absorbers, allowing for a cleaner study of the medium's structure.

2.5 Doppler Shift and Velocity Measurements

One of the key tools in understanding the dynamics of galaxies and their gaseous environments is the Doppler effect. When atoms or molecules in a galaxy absorb or emit light, the wavelengths of these spectral lines can appear shifted due to the relative motion between the source and the observer.

2.5.1 Redshift and Blueshift

If the source of light is moving away from the observer, the spectral lines appear shifted toward longer wavelengths, a phenomenon known as redshift. Conversely, if the source is moving toward the observer, the lines shift toward shorter wavelengths, known as blueshift. In astrophysics, these shifts are quantified using the redshift parameter z, defined as:

$$z = \frac{\lambda_{\text{obs}} - \lambda_{\text{rest}}}{\lambda_{\text{rest}}}$$

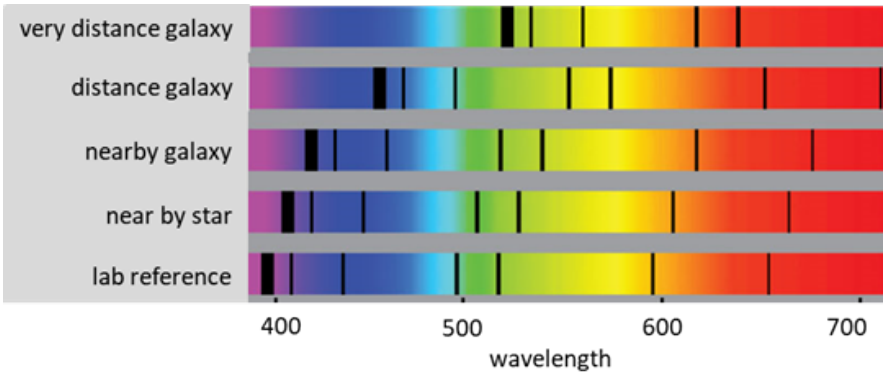

Figure 4: Progressive redshift of spectral lines observed in galaxies at increasing distances compared to a laboratory reference. This shift is used to calculate the velocity of gas and galaxies relative to Earth.
[14]

where λ_{obs} is the observed wavelength, and λ_{rest} is the rest-frame wavelength of the spectral line.

2.5.2 Velocity Calculation

The velocity of the absorbing or emitting gas relative to the observer can be estimated from the redshift using the relativistic Doppler formula. However, for non-relativistic speeds (much less than the speed of light), a simpler linear approximation suffices:

$$v \approx c \cdot \frac{\lambda_{\text{obs}} - \lambda_{\text{rest}}}{\lambda_{\text{rest}}}$$

where v is the velocity and c is the speed of light.

This velocity shift is particularly useful in analyzing Mg II, Fe II, and O II absorption lines to detect outflows in post-starburst galaxies. A blueshifted Mg II line, for example, implies that gas is moving toward the observer—suggestive of an outflowing wind.

2.5.3 Application in This Thesis

In this work, velocity shifts are calculated for Mg II absorption features in both galaxy and quasar spectra. By comparing observed wavelengths to the expected values based on systemic redshifts, we assess whether the gas is moving outward (outflow), inward (infall), or is part of an intervening system. The difference in velocity between expected and observed lines is a key diagnostic for interpreting the origin of absorption features in post-starburst environments.

2.6 Sloan Digital Sky Survey (SDSS)

The Sloan Digital Sky Survey (SDSS) is one of the most ambitious and influential astronomical surveys ever undertaken. Since its launch in 2000, SDSS has mapped over one-third of the sky, producing detailed images and spectra of millions of celestial objects, including stars, galaxies, and quasars. Its multi-phase design has allowed successive upgrades in instrumentation and scope, enabling high-precision studies of cosmic structure, galaxy evolution, and the large-scale distribution of matter in the universe [5].

SDSS uses a dedicated 2.5-meter wide-angle optical telescope at Apache Point Observatory in New Mexico. It is equipped with a sophisticated multi-fiber spectrograph capable of obtaining spectra for hundreds of objects simultaneously. The telescope collects light which is dispersed through gratings to produce high-resolution spectra, typically covering wavelengths from about 3800 Å to 9200 Å [1].

2.6.1 SDSS Data Products and Use in This Thesis

Spectroscopic data from SDSS includes flux as a function of wavelength, redshift estimates, classification (e.g., galaxy, QSO), and observational metadata such as signal-to-noise ratio and spectral resolution. These properties make SDSS an ideal tool for large-scale statistical analyses of galaxy populations, AGN activity, and line-of-sight absorption.

In this thesis, SDSS data is utilized to retrieve spectra for both post-starburst galaxies and quasars in their vicinity. Galaxy spectra are used to identify key absorption features like the Mg II doublet and O II lines, while quasar spectra serve as background sources to probe absorption from intervening material. The availability of public SDSS tools (e.g., via Astroquery and the SDSS SkyServer) further simplifies automated spectral retrieval and redshift analysis.

2.7 NASA/IPAC Extragalactic Database (NED)

The NASA/IPAC Extragalactic Database (NED) is a comprehensive astronomical resource dedicated to the collection, cross-identification, and integration of data related to extragalactic objects. Maintained by the Infrared Processing and Analysis Center (IPAC), NED aggregates information from numerous sky surveys, spectroscopic catalogs, and individual studies, allowing astronomers to search for galaxies, quasars, AGNs, and other non-stellar objects across a broad range of wavelengths [9].

One of NED's primary functions is to serve as a cross-matching and classification tool. Each object is linked to multiple identifiers across surveys (e.g., SDSS, 2MASS,

GALEX), and the database provides redshift data, object type classifications, and references to published literature. This integration makes NED especially valuable when trying to verify the nature of sources (e.g., distinguishing quasars from stars or galaxies) and to collect multi-wavelength metadata.

2.7.1 NED in This Thesis

In this thesis, NED is used to identify quasars located near selected post-starburst galaxies. By querying NED for extragalactic sources within a specified radius and filtering results based on type (e.g., QSO, AGN, Seyfert), we ensure that the quasar candidates used for background absorption analysis are properly classified. The redshift information retrieved from NED is also used to determine whether the quasar lies behind the galaxy, which is critical for interpreting any observed absorption as intervening rather than intrinsic.

While NED provides powerful filtering and cross-matching capabilities, it is not without limitations. Some object classifications may be outdated or uncertain, and not all redshifts are spectroscopically confirmed. As such, further verification using SDSS data or other catalogs is often necessary when precision is required.

3 Method

3.1 Data Selection and Preparation

This study focuses on analyzing optical spectroscopic data from the Sloan Digital Sky Survey (SDSS), targeting post-starburst galaxies and background quasars. The post-starburst systems were selected based on their E+A classification, featuring strong Balmer absorption lines and little to no [O II] or H α emission — indicative of a recent, rapidly quenched starburst phase. Initial targets were chosen based on galaxies discussed in Tremonti et al. (2007) [17].

At the outset, the primary goal was to analyze the spectral properties of post-starburst galaxies themselves. Attention was placed on identifying features such as Mg II and O II lines, and determining whether they showed signs of kinematic shifts consistent with galactic outflows. This involved detailed continuum normalization and velocity shift analysis. However, as more galaxies were examined, it became increasingly important to determine whether the observed absorption was intrinsic to the galaxies or influenced by intervening circumgalactic or intergalactic material.

To resolve this ambiguity, quasars were introduced into the analysis as background light sources. The initial method for identifying quasars was a brute-force, manual approach: each galaxy was visualized in the ALADIN sky atlas, and quasars were selected by visually inspecting SDSS overlays. Their coordinates were manually extracted, and the corresponding spectra were downloaded individually from the SDSS archive. While this method seemed straightforward and manageable for a small number of systems, it quickly became time-consuming and inefficient as more galaxies were studied.

To address this, the selection process was refined using the NASA/IPAC Extragalactic Database (NED). A script was developed to automate the search for nearby extragalactic objects within a 10 arcminute radius of each galaxy. Results were filtered to include only sources classified as QSO, AGN, BLAGN, or Seyfert. An additional redshift filter — requiring $z_{\mathrm{QSO}} > z_{\mathrm{gal}} - 0.1$ — was applied to ensure that quasars were sufficiently behind the galaxy to act as effective absorption probes.

For all verified quasars and galaxies, spectral data was retrieved from SDSS using spectroscopic metadata (plate, MJD, fiberID). Each spectrum was saved as a FITS file and prepared for further processing in Python.

3.2 Spectral Processing

The spectra of both post-starburst galaxies and quasars were obtained from the Sloan Digital Sky Survey (SDSS) in FITS format. Each spectrum contains the flux as a

function of wavelength, along with observational metadata such as redshift and object classification. All spectra were processed using Python libraries including `Astropy`, `Specutils`, and `Matplotlib`.

The first step was to convert the SDSS wavelength grid, which is provided in logarithmic units, into linear space. The flux values were also scaled according to SDSS flux calibration (typically in units of 10^{-17} erg s^{-1} cm^{-2} Å^{-1}). Once the wavelength and flux arrays were prepared, they were used to construct `Spectrum1D` objects, which allowed for further analysis.

To identify line features, it was essential to normalize the continuum. A third-degree polynomial was fit to the spectra using the `fit_continuum` method from `Specutils`. In many cases, certain wavelength regions were masked to avoid fitting over strong emission or absorption lines, as well as to mitigate the effects of noise spikes. This masking was done either manually or by defining conservative regions to exclude from the fit.

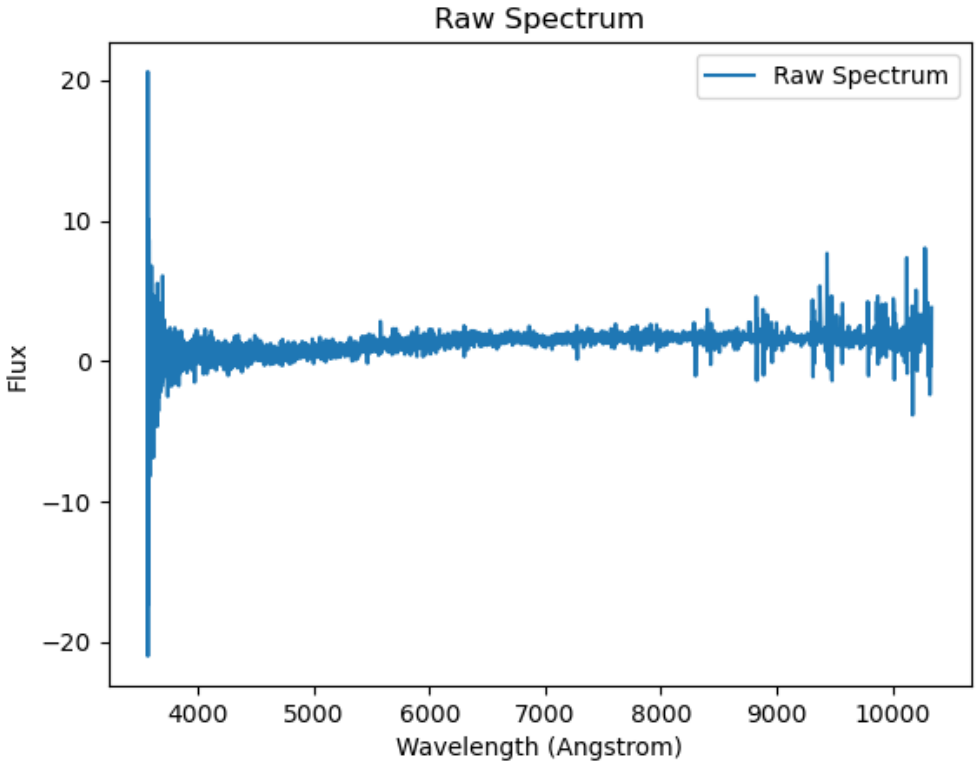

Figure 5: Example of a raw SDSS spectrum loaded for a post-starburst galaxy. The flux is shown before continuum normalization or noise clipping.

After fitting, each spectrum was divided by its continuum model to produce a normalized spectrum. Because normalization could sometimes produce extreme values in regions of high noise, the resulting normalized flux was clipped to a defined range (e.g.,

$[-60, 60]$) for visualization. The normalized spectra were then plotted with labeled axes and expected line markers to prepare for detailed absorption line analysis.

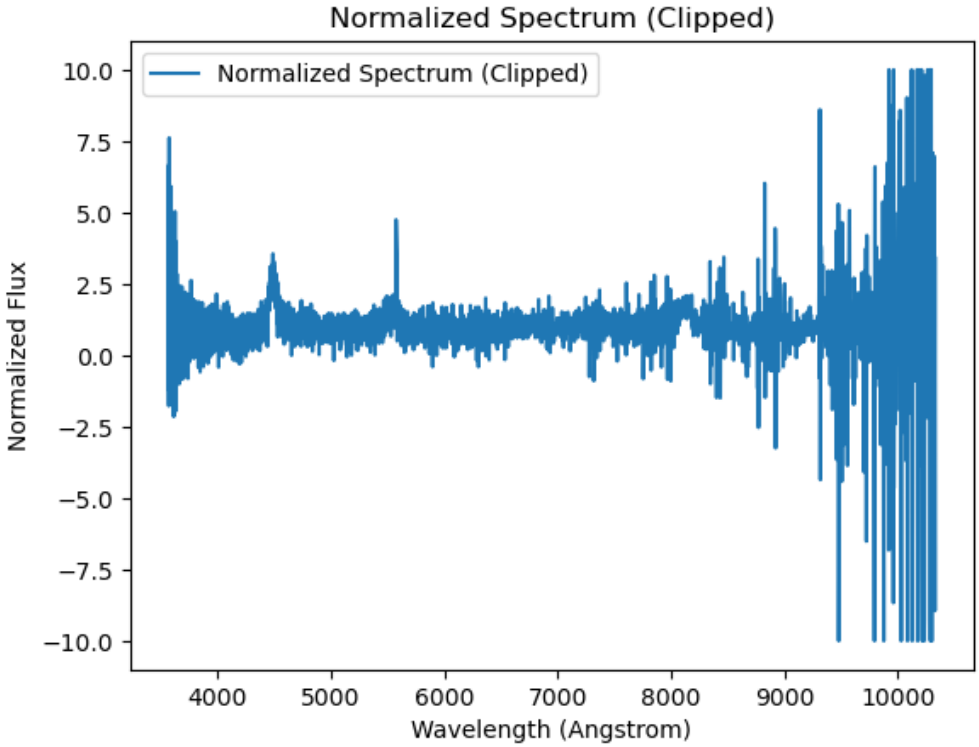

Figure 6: Clipped and continuum-normalized spectrum of the same object. Prominent absorption features are more clearly visible after preprocessing.

These normalized and clipped spectra served as the foundation for all subsequent steps, including Doppler shift calculations and comparisons between galaxy and quasar sightlines.

3.3 Redshift Handling

Accurate redshift determination was essential for analyzing the kinematic properties of spectral lines and ensuring that quasars used as background sources were located behind the target galaxies. For each post-starburst galaxy, the redshift (z_{gal}) was retrieved directly from SDSS metadata. These values were generally robust, as they were derived from spectral line fitting during the SDSS pipeline reduction.

For quasars, two approaches were used to determine redshifts. Initially, redshifts were obtained from the SDSS query results based on coordinates. However, to enhance the reliability of classification and redshift consistency, the selection process was later refined using the NASA/IPAC Extragalactic Database (NED). NED not only provided object types (e.g., QSO, AGN, Seyfert) but also included spectroscopically derived

redshifts, which were cross-checked against SDSS results.

A filtering condition was applied to include only those quasars that satisfied:

$$z_{\mathrm{QSO}} > z_{\mathrm{gal}} - 0.1$$

This buffer was chosen to account for uncertainties in redshift estimation and to ensure that the quasar lay sufficiently behind the galaxy along the line of sight. This allowed for the investigation of potential intervening absorption features in the quasar spectrum that could be attributed to the circumgalactic medium (CGM) of the foreground galaxy.

The confirmed redshifts were then used to calculate the rest-frame positions of spectral lines (e.g., Mg II, O II, Fe II) for both galaxy and quasar spectra. To quantify the velocity difference between observed and expected line positions, the Doppler velocity shift formula was applied:

$$v = c \cdot \frac{\lambda_{\mathrm{obs}} - \lambda_{\mathrm{exp}}}{\lambda_{\mathrm{exp}}}$$

where λ_{obs} is the observed wavelength of a line, λ_{exp} is its expected wavelength based on the redshift, and c is the speed of light. This calculation was used extensively in both galaxy and quasar spectra to interpret blueshifts and redshifts as signatures of outflows or absorption.

3.4 Mg II Doublet Analysis

The Mg II resonance doublet, consisting of absorption lines at 2796 Å and 2803 Å, is a prominent feature in many galaxy and quasar spectra. These transitions are particularly sensitive to low-ionization, cool gas and are commonly used to trace galactic-scale outflows and circumgalactic medium (CGM) structures. Because of their strength and frequency of detection in UV/optical spectra, they are ideal probes of the gas kinematics in and around galaxies.

To analyze potential velocity shifts of the Mg II lines, the normalized quasar spectra were carefully examined around the redshifted expected positions of the doublet. These expected wavelengths were calculated using the known redshift of each quasar (obtained from NED/SDSS), using the formula:

$$\lambda_{\mathrm{expected}} = \lambda_{\mathrm{rest}} \times (1 + z)$$

In practice, absorption lines do not always appear exactly at the expected redshifted positions. Line shifts, particularly blueshifts, may indicate that gas is moving toward

the observer, such as in the case of galactic winds. In this study, observed wavelengths for the Mg II 2796 Å and 2803 Å lines were determined manually by visual inspection — the deepest absorption troughs near the expected wavelengths were selected as the observed positions.

Importantly, the spectra used for this analysis were already corrected for the systemic redshift of the galaxy. Therefore, any measured blueshift in the Mg II lines is interpreted as a velocity offset relative to the galaxy's rest frame. This ensures that the velocity shift reflects real gas motions (e.g., outflows) rather than cosmological redshift effects.

As an illustrative example, the Mg II region in spectra of the galaxy J150636.30+540220.9 is shown in Figures 7 and 8. In Figure 7, the spectrum is centered around the calculated expected positions based on the quasar redshift. In Figure 8, vertical solid lines mark the actual absorption troughs observed in the data. The discrepancy between expected and observed wavelengths highlights the presence of blueshifted absorption, consistent with fast outflowing gas.

For this particular example:

- The expected wavelength for the Mg II 2796 Å line was 4495.56 Å, while the observed minimum occurred at 4481.50 Å, resulting in a velocity shift of **-937.54 km/s**.
- The Mg II 2803 Å line was expected at 4506.81 Å, with the observed absorption at 4490.40 Å, giving a velocity shift of **-1091.85 km/s**.

These velocities were calculated using the classical Doppler formula:

$$v = c \cdot \frac{\lambda_{\text{observed}} - \lambda_{\text{expected}}}{\lambda_{\text{expected}}}$$

where c is the speed of light in vacuum.

This analysis demonstrates the effectiveness of the Mg II doublet as a tracer of cool, fast-moving gas. The strong blueshifts observed in several spectra (with this one shown as a representative case) provide strong evidence for the presence of large-scale outflows in the galaxies under study — a key diagnostic when interpreting the connection between post-starburst galaxies and feedback-driven gas dynamics.

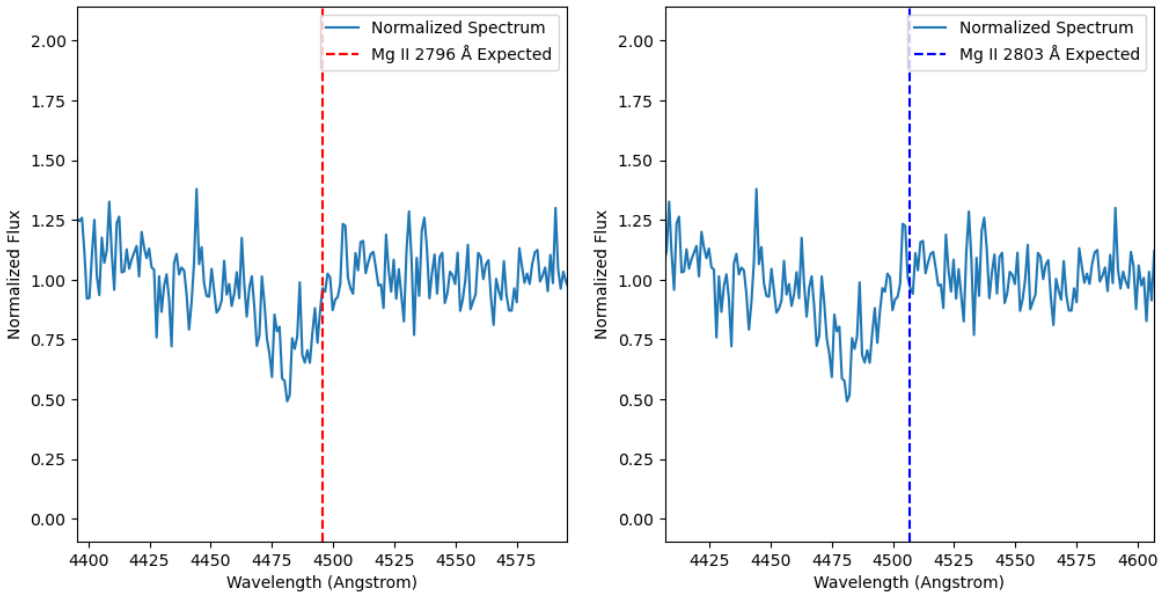

Figure 7: Zoomed-in view of normalized spectra near the **expected** redshifted positions of the Mg II 2796 Å (left) and 2803 Å (right) lines. Dashed lines mark the expected positions based on galaxy redshift.

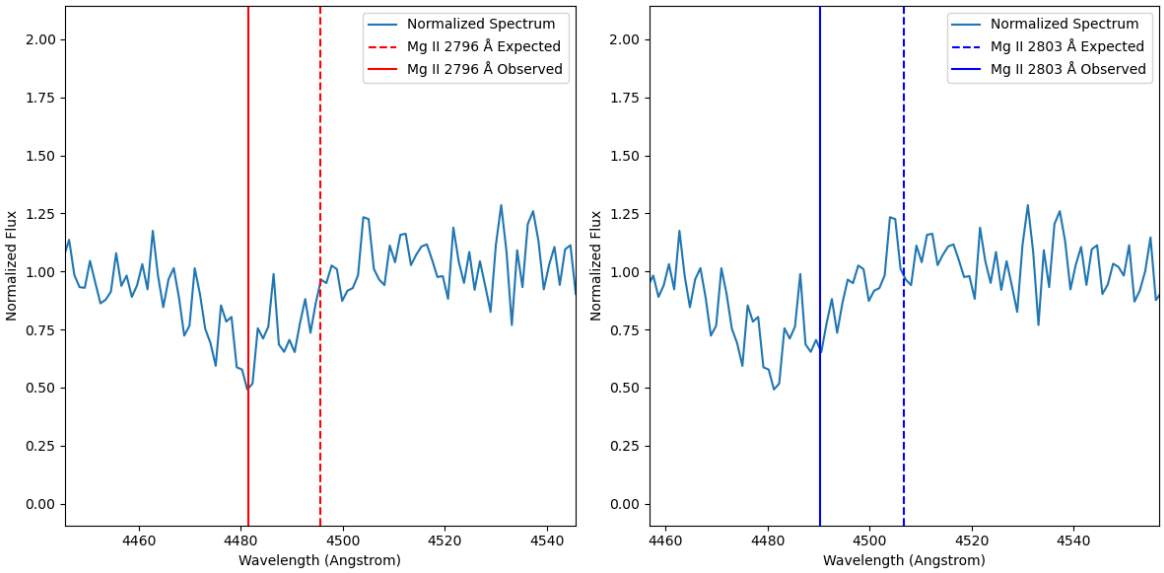

Figure 8: Zoomed-in view of the same spectra showing the **observed** Mg II absorption minima (solid lines). The observed wavelengths were selected manually by visual inspection, showing significant blueshifts from the expected positions.

3.5 [O II] Doublet Analysis

In addition to Mg II, the [O II] emission doublet at 3726 Å and 3729 Å was also examined in the normalized spectra of galaxies and quasars. These lines, typically associated with ionized gas in star-forming regions, can also offer insights into gas dynamics and the presence of inflows or outflows.

The analysis followed the same approach as for Mg II: the expected wavelengths were calculated based on the redshift, and the spectral region was visually inspected for corresponding features. Since the [O II] lines are often weaker and more sensitive to noise or instrumental resolution, no velocity shifts were quantitatively estimated for this work.

Nevertheless, the presence or absence of [O II] absorption or emission helped provide context for the interpretation of other lines and supported classification of the galaxy's activity state.

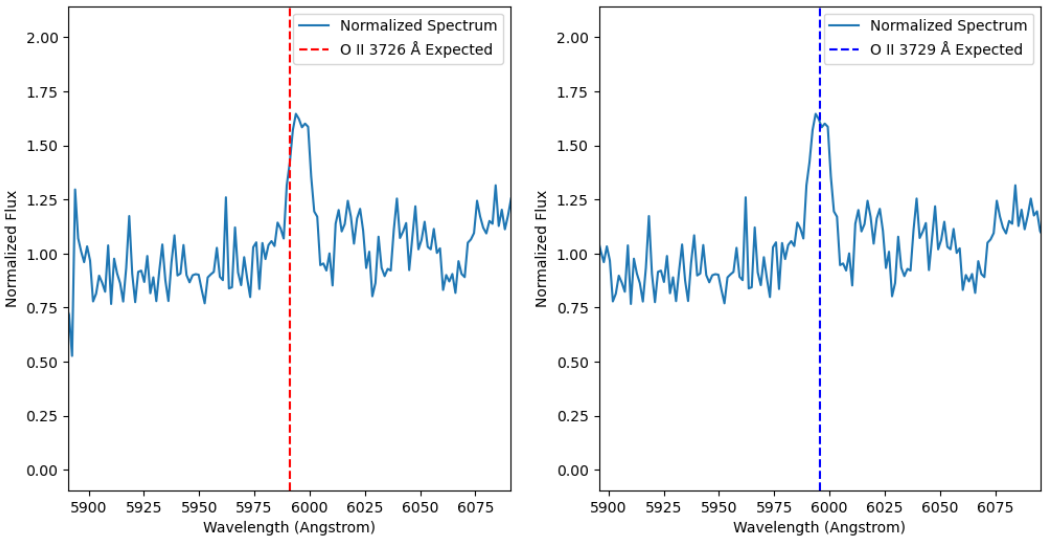

Figure 9: Example of [O II] doublet region in a normalized spectrum. Dashed lines mark expected positions based on redshift.

3.6 Data Access Tools: SDSS and NED

Sloan Digital Sky Survey (SDSS)

The Sloan Digital Sky Survey (SDSS) is a large-scale spectroscopic and imaging survey that has been instrumental in modern astrophysics. It provides access to high-resolution optical spectra for millions of objects, including galaxies and quasars. In this project, SDSS served as the primary source for acquiring both galaxy and quasar spectra.

Spectra were accessed programmatically using the `Astroquery.sdss` module in Python. Each spectrum includes calibrated flux, logarithmic wavelength arrays, and metadata such as redshift, plate ID, MJD, and fiber number. These were essential for redshift determination, normalization, and spectral line analysis.

NASA/IPAC Extragalactic Database (NED)

NED was used to verify object classifications and retrieve additional redshift and metadata information, especially for quasars. Unlike SDSS, which does not explicitly label quasars as such in every case, NED provides object type labels such as QSO, AGN, Seyfert, and BLAGN. This classification was critical in filtering valid background quasar candidates.

NED queries were conducted using the `Astroquery.ned` interface. Objects were filtered based on proximity (within a 10 arcminute radius) to post-starburst galaxies and redshift criteria ensuring that the quasar lay behind the galaxy along the line of sight. Cross-matching NED with SDSS allowed both identification and spectral acquisition.

Together, SDSS and NED provided a complementary framework: SDSS for spectral data and redshift measurement, and NED for object classification and quasar verification.

3.7 Quasar–Galaxy Spatial Geometry

To evaluate whether Mg II absorption in quasar spectra could be linked to the foreground post-starburst galaxy, the angular distance between each quasar and the galaxy was measured. Right Ascension (RA) and Declination (Dec) coordinates were retrieved from NED for each background quasar. The angular separation was calculated using astrometric tools based on spherical geometry.

To interpret these angular distances in physical units, they were converted to projected transverse distances using the angular diameter distance corresponding to each galaxy's redshift. For a typical system at redshift $z \approx 0.516$, the angular diameter distance is approximately 1319 Mpc, assuming a standard ΛCDM cosmology ($H_0 = 70\,\mathrm{km\,s^{-1}\,Mpc^{-1}}$, $\Omega_m = 0.3$, $\Omega_\Lambda = 0.7$). At this redshift, 10 arcminutes corresponds to a physical separation of roughly 3.8 Mpc.

As an illustrative example, the figure below shows the relative positions of one post-starburst galaxy (red star) and three surrounding quasars (blue circles). The quasars are labeled QSO 1 through QSO 3 based on their order in analysis. Their spatial separation varies from approximately 3.2 to 3.7 Mpc in projected distance. Notably,

QSO 3, which lies closest to the galaxy, showed hints of Mg II absorption, whereas the more distant quasars did not.

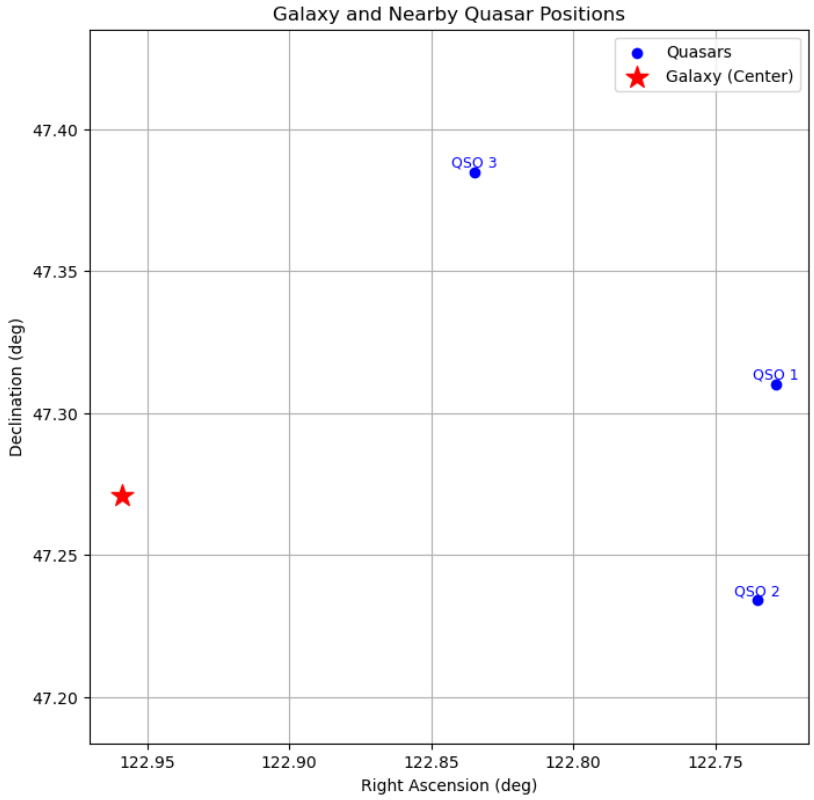

Figure 10: Sky plot showing the position of the post-starburst galaxy (red star) and nearby quasars (blue points), labeled QSO 1 to QSO 3. All objects are plotted in RA and Dec using equatorial coordinates.

4 Results

A sample of post-starburst galaxies was selected from the SDSS database, and corresponding background quasars were identified within a 10 arcminute radius using NED cross-matching. For each galaxy–quasar pair, Mg II $\lambda\lambda$2796, 2803 Å absorption features were analyzed in both the galaxy and quasar spectra. All wavelengths were converted to the rest frame of the galaxy using its spectroscopic redshift.

In the galaxy spectra, blueshifted Mg II absorption was commonly observed. The expected wavelengths of the Mg II doublet, based on the galaxy redshift, were compared to the visually identified absorption troughs. Velocity shifts were calculated using the Doppler formula and typically ranged between few hundred to over thousand $\mathrm{km\,s^{-1}}$, consistent with fast-moving gas.

In contrast, the analysis of Mg II in background quasar spectra yielded fewer clear detections. In many cases, no significant absorption was observed at the expected positions. A few quasars exhibited weak features near the Mg II positions, but these were often redshifted relative to the galaxy rest frame rather than blueshifted. This suggests they are not likely to originate from outflowing material associated with the foreground galaxy. In a small number of cases, broad features resembling emission rather than absorption were observed in regions where Mg II absorption might have been expected.

The presence or absence of absorption did not strongly correlate with angular separation. Some of the quasars closest to the galaxy in projection (within few hundred kpc) still lacked clear Mg II absorption, while others more distant showed weak features. These findings suggest that either the absorbing gas is highly anisotropic and clumpy, or the features are unrelated to the post-starburst galaxy.

The following sections present example systems that illustrate these trends, including observed spectra, measured wavelength shifts, and spatial plots in RA/Dec and physical projected distance.

4.1 Representative Galaxy–Quasar Systems

The following subsections present few representative systems that illustrate the diversity of spectral features observed in the quasar spectra. Both systems involve post-starburst galaxies with clearly blueshifted Mg II absorption lines, consistent with galactic outflows. However, the associated quasar spectra show unexpected behaviors, including possible redshifted absorption features and, in rare cases, an emission-like profile in the Mg II region. These examples highlight the complexity of interpreting line-of-sight absorption and the challenges in attributing it directly to the foreground

galaxy.

System 1: J155811.27+395720.7

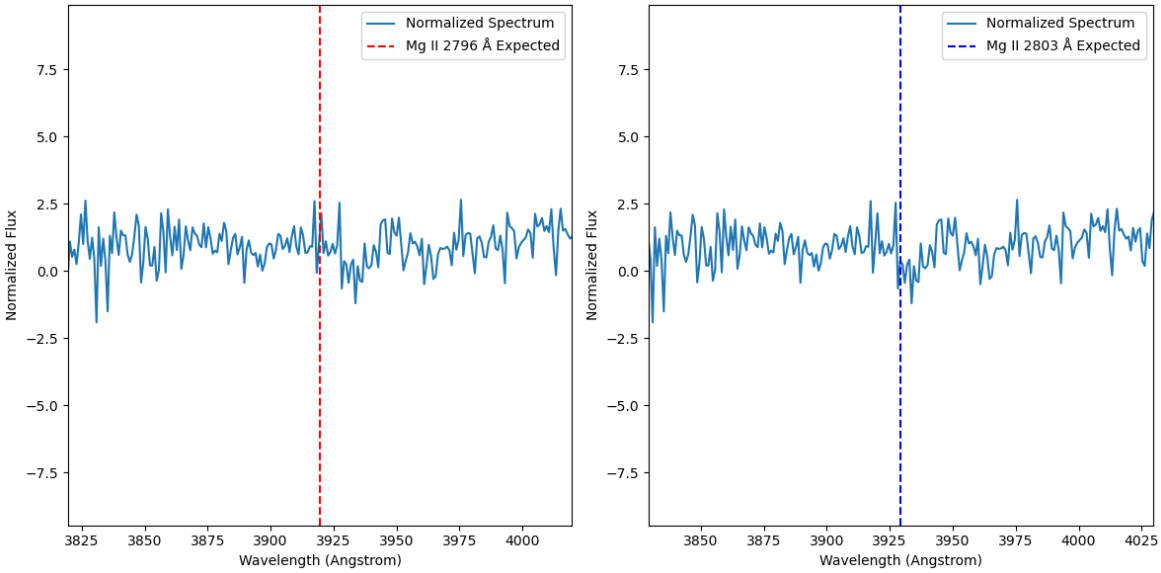

Figure 11: Normalized spectrum background quasar near galaxy J155811.27+395720.7 in the Mg II region. Dashed lines indicate expected doublet positions based on the galaxy redshift.

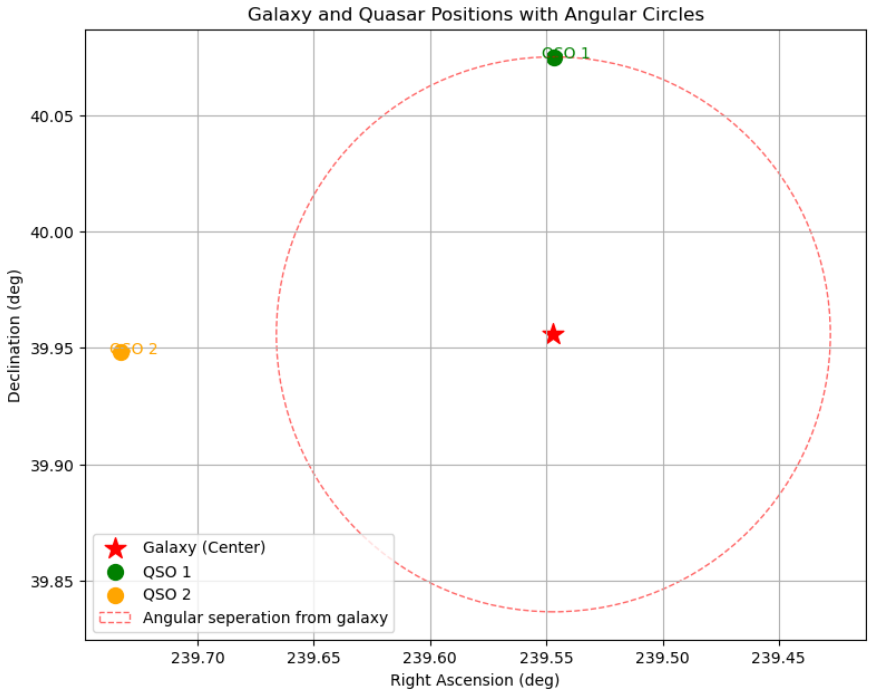

Figure 12: RA and Dec plot of galaxy J155811.27+395720.7 and nearby quasars. Circles indicate angular separation from the galaxy.

This galaxy exhibits blueshifted Mg II absorption consistent with outflowing gas. However, in the spectrum of a nearby quasar, a possible Mg II absorption feature appears redshifted relative to the expected wavelength calculated using the galaxy redshift. No clear blueshifted absorption was detected in the quasar spectrum.

A map of the system in RA and Dec is shown in Figure 12, and the galaxy's Mg II region is plotted in Figure 11.

System 2: J150636.30+540220.9

This galaxy, which was also used as an example in the Methods section, shows clear blueshifted Mg II absorption in its own spectrum. In the spectrum of a nearby background quasar, however, a possible Mg II absorption feature appears redshifted relative to the expected position. Additionally, the galaxy spectrum displays a broad emission-like bump in the Mg II region, centered slightly blueward of the expected absorption. These features were identified visually in the normalized spectra.

This combination of redshifted absorption in the quasar spectrum and unusual emission-like structure in the galaxy spectrum suggests a more complex or asymmetric structure in the outflowing or intervening medium.

Figures 13 and 15 show the relevant spectra and spatial geometry.

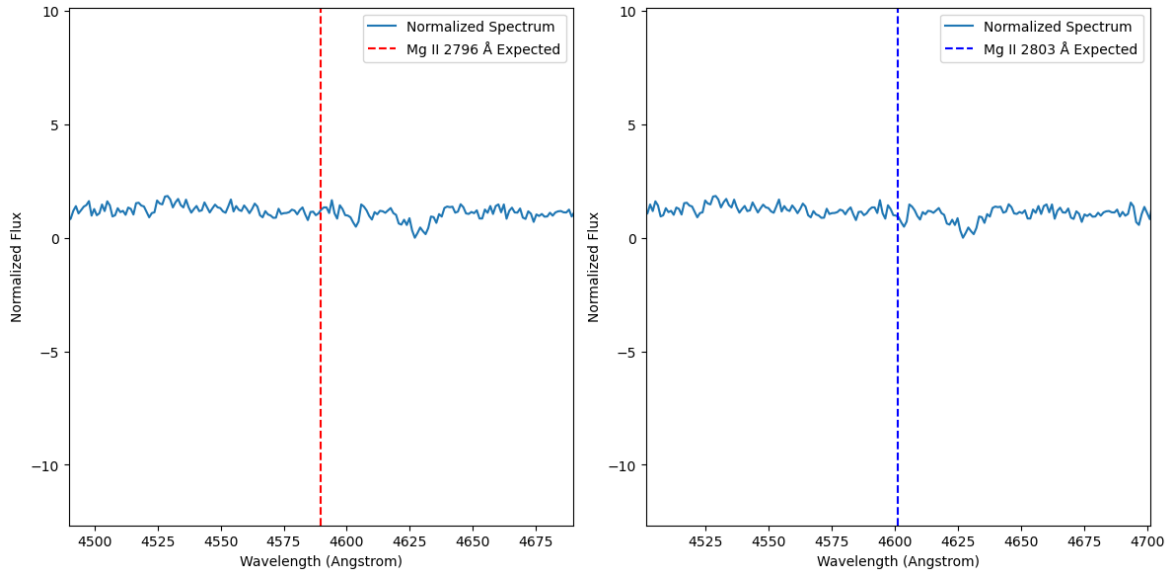

Figure 13: Normalized spectrum of background quasar near galaxy J150636.30+540220.9 in the Mg II region. A redshifted absorption-like feature and is visible.

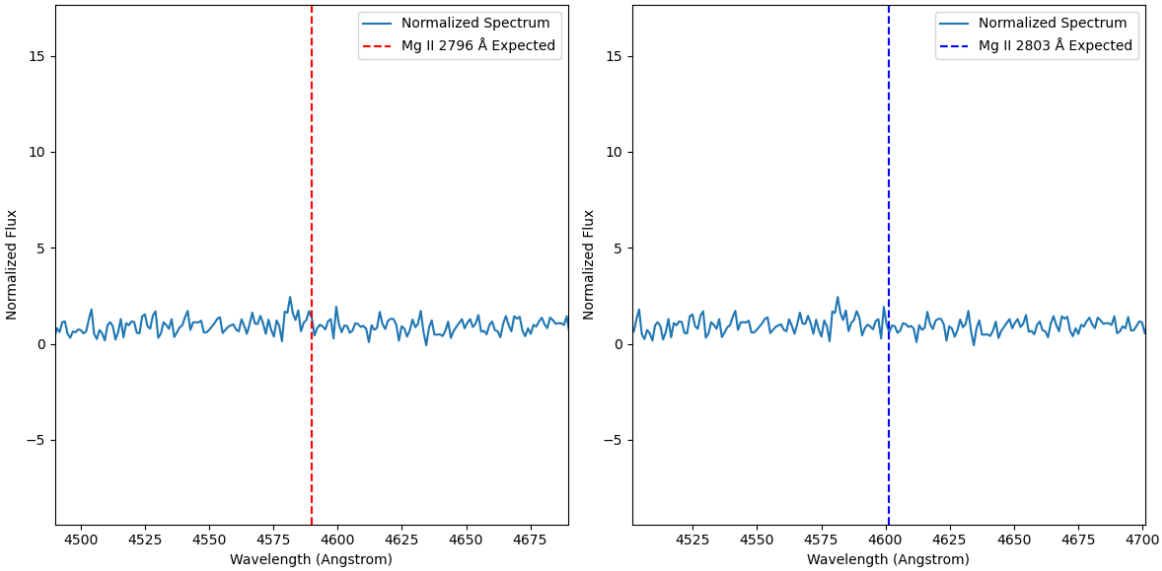

Figure 14: Normalized spectrum of background quasar near galaxy J150636.30+540220.9 in the Mg II region, a blueshifted emission-like structure is visible.

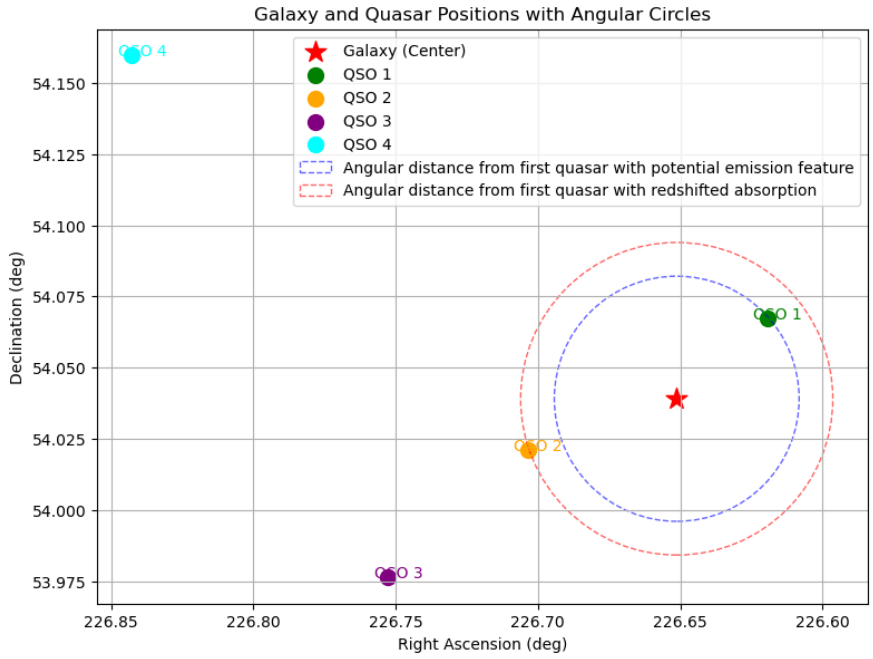

Figure 15: RA and Dec plot of galaxy J150636.30+540220.9 and associated quasars. One nearby quasar shows a possible redshifted Mg II absorption feature.

System 3: J161332.51+283414.5

In this system, the galaxy spectrum again shows clearly blueshifted Mg II absorption, consistent with the presence of outflowing gas. A nearby background quasar was analyzed for signs of Mg II absorption at the expected wavelength based on the galaxy's redshift.

The quasar spectrum shows a possible absorption feature near the Mg II doublet position; however, the signal-to-noise ratio in this region is relatively low, making it difficult to confidently determine the presence or precise velocity offset of the line. Although the feature appears to be near the expected wavelength, the uncertainty in its depth and width makes the interpretation ambiguous.

Despite the noise, the spectrum is worth noting as a borderline case where absorption may be present but is not significant enough to classify as a confident detection.

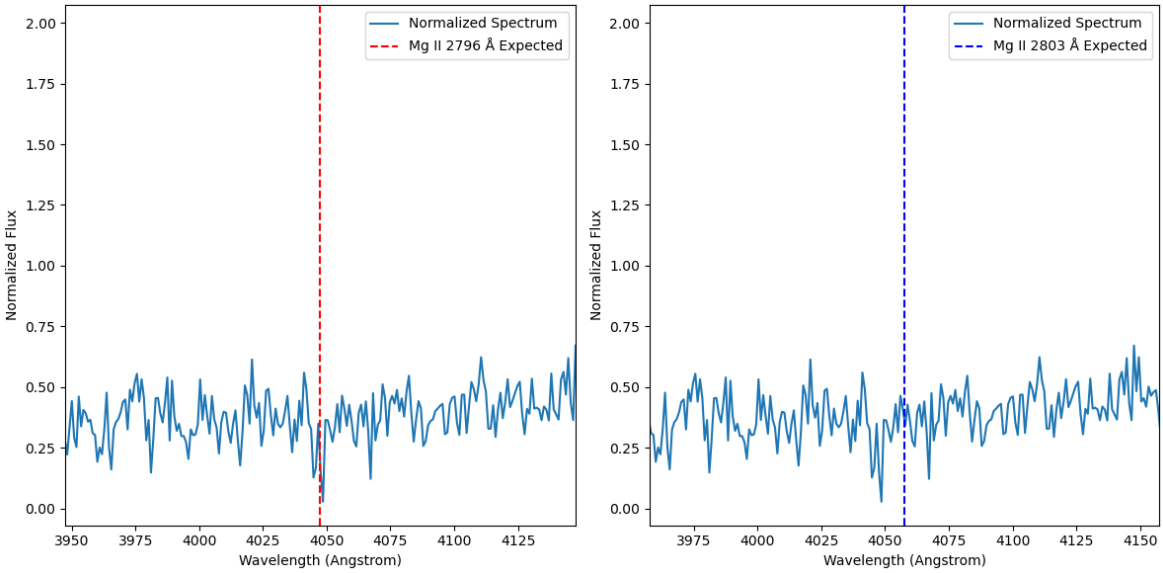

Figure 16: Normalized spectrum of a background quasar near galaxy J161332.51+283414.5 in the Mg II region. A possible absorption feature is seen near the expected wavelength, though high noise limits confidence.

5 Conclusion

The goal of this work was to investigate whether Mg II absorption observed in post-starburst galaxy spectra is also detectable in the spectra of background quasars within a projected distance of up to ∼3.8 Mpc. Such detections would potentially indicate the presence of extended outflows or circumgalactic medium (CGM) structures associated with these galaxies.

Multiple post-starburst galaxies in the sample did show clear blueshifted Mg II absorption, with velocity offsets ranging from several hundred to over 1000 $\mathrm{km\,s^{-1}}$. This is consistent with expectations for galaxies undergoing feedback-driven winds following a recent starburst episode. These findings align with prior studies associating the post-starburst phase with large-scale gas ejection driven by AGN activity or supernova feedback.

In contrast, Mg II absorption was rarely observed in the spectra of background quasars near these galaxies. In a few cases, potential absorption features were detected, but these were typically redshifted relative to the galaxy redshift—making them inconsistent with a simple outflow scenario. One quasar spectrum even exhibited an emission-like bump near the expected absorption position, further complicating interpretation. The majority of quasar spectra showed no significant absorption at all.

These results suggest that the Mg II-absorbing outflows may be confined to relatively small physical scales—below the several-Mpc range probed by the quasar sightlines—or that the absorbing material is highly anisotropic and clumpy, resulting in a low covering fraction. It is also plausible that some of the redshifted features observed in quasar spectra originate from unrelated foreground or intervening systems along the line of sight.

A contributing limitation to the analysis was the signal-to-noise ratio of many quasar spectra. In several cases, low S/N hindered confident identification of absorption features and may have resulted in missed detections. Additionally, differences in redshift and line-of-sight geometry between quasars and galaxies introduce further complexity in interpreting absorption features.

Overall, while the galaxy spectra confirm the presence of strong outflows through blueshifted Mg II absorption, the lack of corresponding features in quasar sightlines suggests these outflows may not extend far into the CGM or are directionally constrained. These findings motivate further investigation using higher S/N quasar spectra, denser background source sampling, and comparison to simulations of feedback-driven gas flows around transitioning galaxies.

6 Limitations and Outlook

While the analysis in this thesis offers a first look into Mg II absorption around post-starburst galaxies using background quasars, several limitations shaped the scope and sensitivity of the results. The most immediate constraint was the relatively low signal-to-noise ratio in many of the available quasar spectra. In several cases, potential absorption features were difficult to confirm due to the noise level, and weaker signals may have remained undetected altogether. Techniques such as spectral stacking or transformation into the frequency domain could help mitigate this issue in the future, enhancing the detectability of subtle absorption features.

Another limitation was the sparse sampling of background quasars. Although a 10 arcminute search radius was used for each galaxy, most systems only had one or two usable quasars in that region. This limited the spatial coverage and made it difficult to draw conclusions about the angular extent or covering fraction of any outflowing or circumgalactic gas. A denser field of background sources—ideally spanning a wider angular range and range of impact parameters—would allow for better geometric characterization of absorption features and their correlation with projected distance.

All line identifications in this study were performed manually through visual inspection. While this approach allowed flexibility and careful attention to borderline cases, it also introduces a level of subjectivity and limits reproducibility. In future work, the use of automated line-finding algorithms or fitting routines would improve consistency, allow for more rigorous statistical analysis, and make large-scale application more feasible.

A key opportunity for future research lies in the availability of higher-quality spectral datasets. While this work relied primarily on SDSS data, the recent first data release of the Dark Energy Spectroscopic Instrument (DESI) dramatically expands the landscape. DESI DR1 includes over 1.5 million quasar spectra with higher signal-to-noise ratios and greater spectral resolution, ranging from $R \sim 2000$ at 360 nm to $R \sim 5500$ at 980 nm. Although this data became available too late for inclusion in this thesis, it presents a major opportunity to revisit this analysis with greatly improved sensitivity. With DESI, it becomes possible not only to detect weaker Mg II absorbers more reliably, but also to conduct statistically significant studies across larger samples with multiple background sightlines per galaxy.

In addition to that, future work could perhaps benefit from integration with simulated data. Cosmological simulations such as FIRE, IllustrisTNG, and EAGLE now include sophisticated models of gas feedback, outflows, and metal-line absorption, and generate mock absorption spectra along random sightlines. Comparing observational results with such models would provide theoretical context and help determine whether

observed features arise from starburst-driven winds, AGN activity, or unrelated structures in the circumgalactic and intergalactic media.

Altogether, this study establishes a foundation for connecting post-starburst galaxies and surrounding gas absorption, while highlighting the need for higher-quality data, better spatial sampling, and more scalable analysis tools. With the growing availability of deeper spectroscopic surveys and high-resolution simulations, future work will be well-positioned to address these challenges and further illuminate the role of feedback and gas dynamics in galaxy evolution.

References

[1] Romina Ahumada, Carlos Allende Prieto, Andres Almeida, et al. "The 16th Data Release of the Sloan Digital Sky Surveys: First Release from the APOGEE-2 Southern Survey and Full Release of eBOSS Spectra". In: *The Astrophysical Journal Supplement Series* 249.1 (2020), p. 3. DOI: 10.3847/1538-4365/ab929e. URL: https://arxiv.org/abs/1912.02905.

[2] Max Planck Institute for Astrophysics. *The Mg II Doublet as a New Tool to Study Cold Gas in Galaxies*. 2024. URL: https://www.mpa-garching.mpg.de/1095088/hl202404.

[3] Ramona Augustin et al. "Clumpiness of Observed and Simulated Cold Circumgalactic Gas". In: *Monthly Notices of the Royal Astronomical Society* 509.4 (2022), pp. 6014–6030. DOI: 10.1093/mnras/stab3332. URL: https://academic.oup.com/mnras/article/509/4/6014/6446326.

[4] Dalya Baron and Hagai Netzer. "Quenching star formation by AGN feedback: the case of post-starburst galaxies". In: *Monthly Notices of the Royal Astronomical Society* 480.1 (2018), pp. 399–410. DOI: 10.1093/mnras/sty1522. URL: https://arxiv.org/abs/1804.03150.

[5] Michael R. Blanton, Matthew A. Bershady, et al. "Sloan Digital Sky Survey IV: Mapping the Milky Way, Nearby Galaxies, and the Distant Universe". In: *The Astronomical Journal* 154.1 (2017), p. 28. DOI: 10.3847/1538-3881/aa7567. URL: https://arxiv.org/abs/1703.00052.

[6] Michael S. Brotherton et al. "Post-Starburst Quasars: A New Class of Active Galaxies". In: *The Astrophysical Journal Letters* 520.1 (1999), pp. L87–L90. DOI: 10.1086/312144. URL: https://ui.adsabs.harvard.edu/abs/1999ApJ...520L..87B.

[7] Yen-Ting Chen et al. "The nature of fast molecular outflows in post-starburst galaxies". In: *arXiv preprint arXiv:2106.05982* (2021). URL: https://arxiv.org/abs/2106.05982.

[8] EurekAlert! Science News. *Hubble sees post-starburst galaxy with dense central gas*. 2022. URL: https://www.eurekalert.org/multimedia/931502.

[9] George Helou, Barry F. Madore, and Michael Schmitz. "The NASA/IPAC Extragalactic Database (NED)". In: *Bulletin of the American Astronomical Society* 23 (1991), p. 90. URL: https://ned.ipac.caltech.edu/.

[10] Ting-Wen Lan and Houjun Mo. "The Circumgalactic Medium of eBOSS Emission Line Galaxies: Signatures of Galactic Outflows in Gas Distribution and Kinematics". In: *The Astrophysical Journal* 866.1 (2018), p. 36. DOI: 10.3847/1538-4357/aadc08. URL: https://www.osti.gov/pages/biblio/1544068.

[11] *MRC 0406-244*. https://en.wikipedia.org/wiki/MRC_0406-244. Accessed April 2025.

[12] ESA NASA and The Hubble Heritage Team (STScI/AURA). *Starburst Galaxy M82 - Hubble Space Telescope Image*. https://esahubble.org/images/opo0614a/. Accessed April 2025. 2006.

[13] National Radio Astronomy Observatory. *Post-Starburst Galaxies Retain Gas but Don't Form Stars*. 2022. URL: https://public.nrao.edu/news/post-starburst-galaxies-gas/.

[14] *Redshift Comparison of Galaxies*. https://astro.unl.edu/naap/hydrogen/redshift.html. Accessed April 2025. 2022.

[15] Kate H. R. Rubin et al. "Extended [O II] Emission as a Signature of Galactic Winds". In: *Astrophysical Journal* 728.1 (2011), p. 55. arXiv: 1710.09195. URL: https://arxiv.org/abs/1710.09195.

[16] ScienceSpace Research Team. *A 100-kiloparsec Wind Feeding the Circumgalactic Medium of a Galaxy*. 2023. URL: https://scispace.com/pdf/a-100-kiloparsec-wind-feeding-the-circumgalactic-medium-of-a-1ktiai5m18.pdf.

[17] Christy A. Tremonti, John Moustakas, and Aleksandar M. Diamond-Stanic. "The Discovery of 1000 km/s Outflows in Massive Poststarburst Galaxies". In: *The Astrophysical Journal Letters* 663.2 (2007), pp. L77–L80. DOI: 10.1086/520082. URL: https://ui.adsabs.harvard.edu/abs/2007ApJ...663L..77T.

[18] Jason Tumlinson, Molly S. Peeples, and Jessica K. Werk. "The Circumgalactic Medium". In: *Annual Review of Astronomy and Astrophysics* 55 (2017), pp. 389–432. DOI: 10.1146/annurev-astro-091916-055240. URL: https://arxiv.org/abs/1709.09180.

[19] Vivienne Wild et al. "The origin of post-starburst galaxies". In: *Monthly Notices of the Royal Astronomical Society* 477.2 (2018), pp. 1708–1728. URL: https://academic.oup.com/mnras/article/477/2/1708/4925584.

[20] Hao-Yi Wu et al. "Post-Starburst Galaxies and Their Long-Lived Outflows". In: *arXiv preprint arXiv:2411.00102* (2024). URL: https://arxiv.org/abs/2411.00102.

A Appendix

A.1 List of Analysed Galaxies

Galaxy	RA (deg)	Dec (deg)	z	Velocity Offset ($\mathrm{km\,s^{-1}}$)
J081150.09+471615.2	122.958720	47.270889	0.515812	-1124
J082638.41+430529.5	126.660030	43.091528	0.513350	-1208
J094417.85+093019.4	146.224365	9.505389	0.347137	-1086
J110437.46+594639.6	166.156095	59.777667	0.731386	-1358
J112518.90+014532.5	171.328750	-1.759028	0.519314	-1334
J124807.16+060111.8	192.030000	6.019950	0.632290	-498
J150636.30+540220.9	226.651250	54.0391386	0.607854	-1015
J214000.49+120914.6	325.002042	12.1540556	0.751408	0
J150603.61+613148.3	226.515076	61.530086	0.436587	-520
J155811.27+395720.7	239.546976	39.955760	0.401866	-815
J161332.51+283414.5	243.385500	28.570698	0.447606	-956

Table 1: Summary of post-starburst galaxies that exhibited distinguishable Mg II absorption. These represent a subset of the full sample, selected based on the presence of visually identifiable absorption features. The listed velocity offset is the average of the measured velocity shifts from both Mg II λ2796 and λ2803 lines. Formal uncertainty estimates are not included due to the visual nature of the line identification.

A.2 List of Analysed Quasars

Quasar	RA (deg)	Dec (deg)	z	Associated Galaxy
J081054.87+471836.5	122.72864	47.31015	3.065	J081150.09+471615.2
J081056.45+471402.6	122.73524	47.23406	1.2087	J081150.09+471615.2
J081120.50+472304.6	122.83488	47.38475	0.6381	J081150.09+471615.2
J082655.68+430449.7	126.73204	43.08050	1.7523	J082638.41+430529.5
J082725.21+430719.0	126.85505	43.12197	1.7013	J082638.41+430529.5
J082730.93+430645.8	126.87889	43.11273	1.5253	J082638.41+430529.5
J082804.70+430449.6	127.01959	43.08045	2.0148	J082638.41+430529.5
J094424.12+092424.4	146.10052	9.40680	1.0226	J094417.85+093019.4
J094459.25+093047.2	146.24688	9.51311	2.0097	J094417.85+093019.4
J112455.27-013753.2	171.23032	-1.63146	1.8179	J112518.90+014532.5
J150628.61+540402.1	226.61923	54.06725	0.6363	J150636.30+540220.9
J150648.87+540116.4	226.70363	54.02123	2.1127	J150636.30+540220.9
J150700.62+535834.9	226.75263	53.97644	1.7365	J150636.30+540220.9
J150722.21+540934.6	226.84258	54.15961	1.5349	J150636.30+540220.9
J150531.82+613547.4	226.38262	61.59652	1.2810	J150603.61+613148.3
J155811.25+400429.5	239.54691	40.07487	1.4923	J155811.27+395720.7
J155855.95+395652.6	239.73314	39.94797	0.4558	J155811.27+395720.7
J161344.89+283014.2	243.43707	28.50397	0.6244	J161332.51+283414.5
J211749.56+001925.7	319.45654	0.32381	5.4473	J211824.05+001729.4
J211816.90+001718.2	319.57044	0.28839	0.8973	J211824.05+001729.4
J211817.39+001316.9	319.57248	0.22137	0.4628	J211824.05+001729.4
J211824.05+001729.4	319.60022	0.29151	0.4589	J211824.05+001729.4
J211849.52+001455.0	319.70639	0.24863	1.8966	J211824.05+001729.4
J211853.35+001712.8	319.72230	0.28690	1.3396	J211824.05+001729.4

Table 2: List of background quasars analyzed in this study, along with their coordinates, redshifts, and the associated foreground post-starburst galaxy near which they were selected.

A.3 Sky Map of All Analyzed Systems

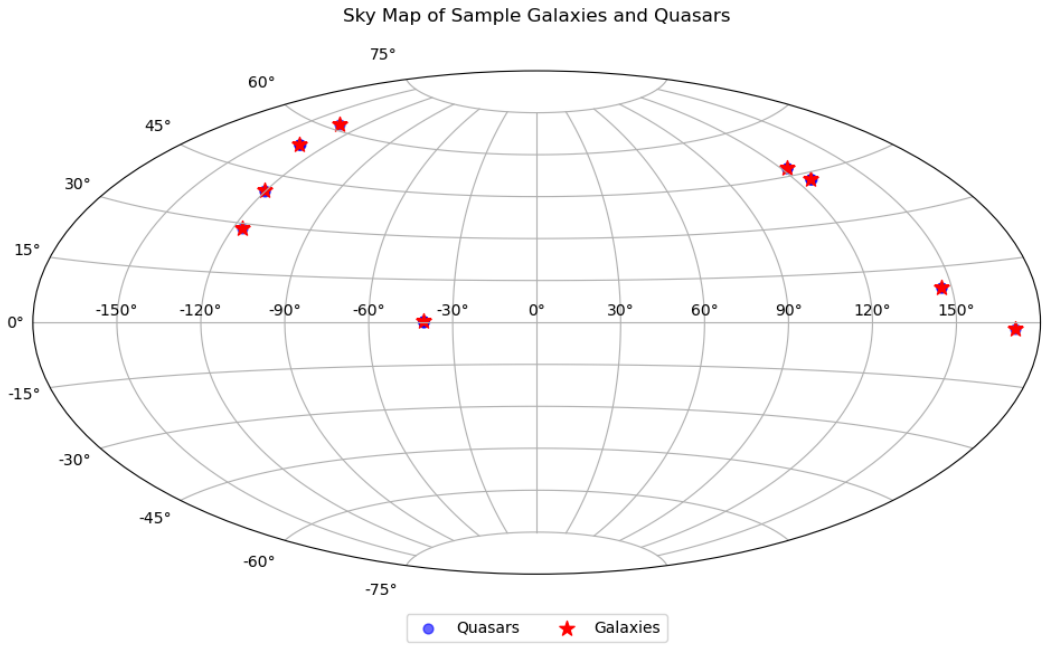

Figure 17: Aitoff projection sky map showing all analyzed galaxies (red stars) and background quasars (blue dots). This map provides a visual overview of the sky coverage of the full sample. Note that, due close proximities of quasar from the galaxies they are overlapping in the whole projection.

A.4 Examples of Mg ii Absorption in Galaxy Spectra

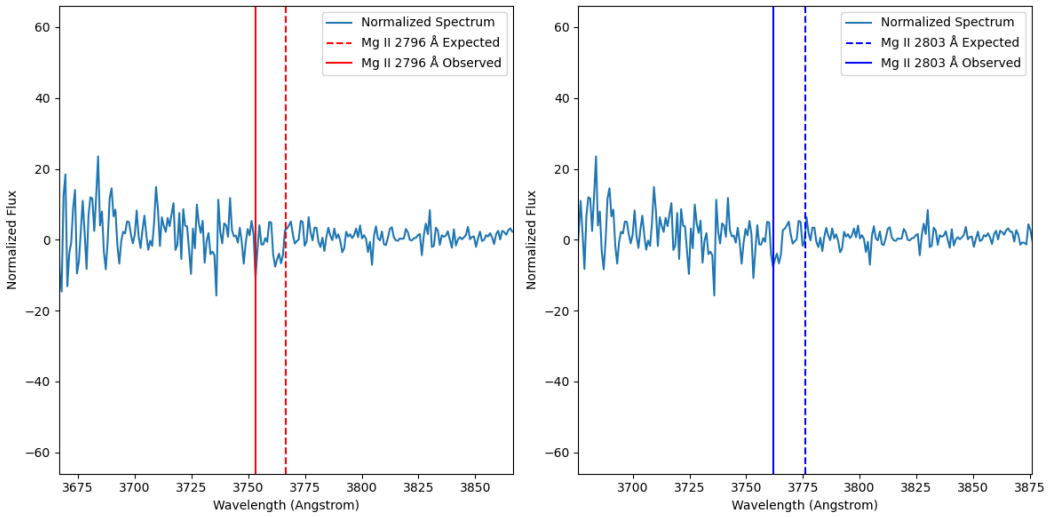

Figure 18: Example 1: Galaxy J094417.85+093019.4 showing clear Mg II $\lambda\lambda$2796, 2803 absorption features. The doublet is blueshifted relative to the expected positions, indicating an outflow with an average velocity offset of $\sim$1086 km s^{-1}.

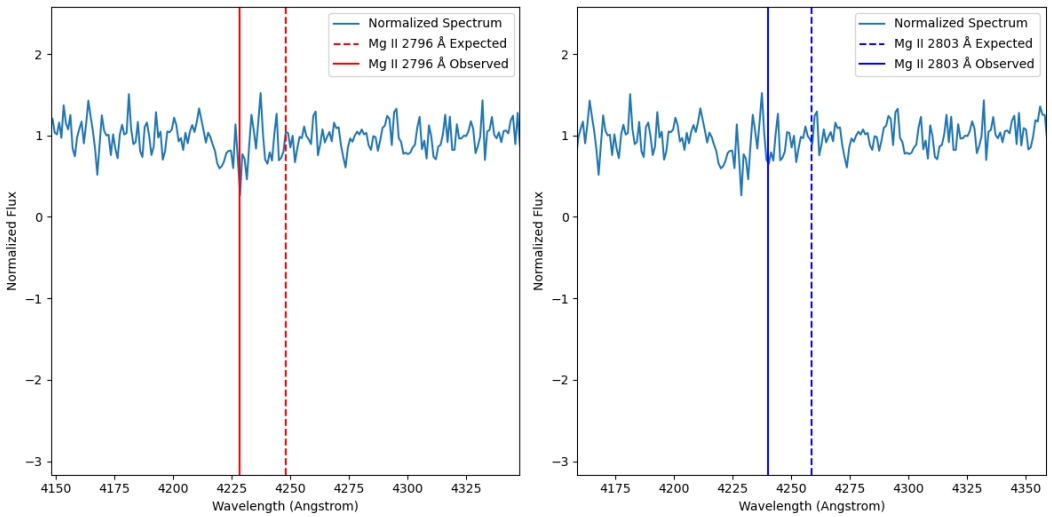

Figure 19: Example 1: Galaxy J112518.90+014532.5 showing clear Mg II $\lambda\lambda$2796, 2803 absorption features. The doublet is blueshifted relative to the expected positions, indicating an outflow with an average velocity offset of $\sim$1334 km s^{-1}.

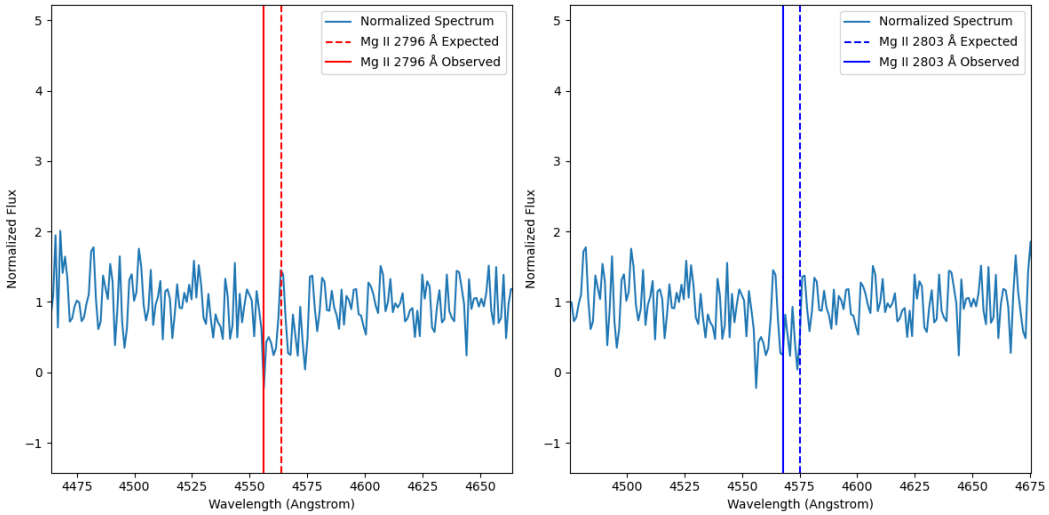

Figure 20: Example 1: Galaxy J124807.16+060111.8 showing clear Mg II $\lambda\lambda$2796, 2803 absorption features. The doublet is blueshifted relative to the expected positions, indicating an outflow with an average velocity offset of $\sim$498 s^{-1}.

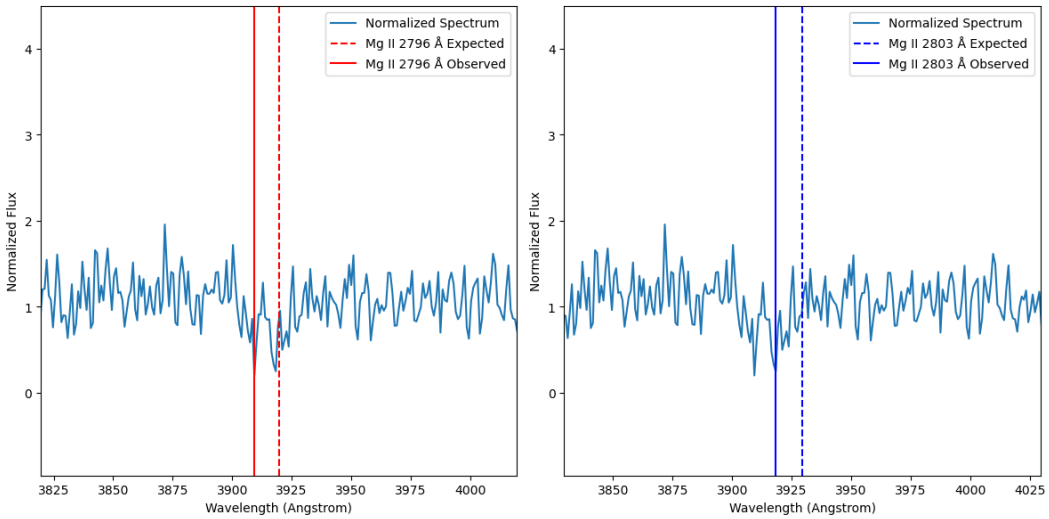

Figure 21: Example 1: Galaxy J155811.27+395720.7 showing clear Mg II $\lambda\lambda$2796, 2803 absorption features. The doublet is blueshifted relative to the expected positions, indicating an outflow with an average velocity offset of $\sim$815 s^{-1}.

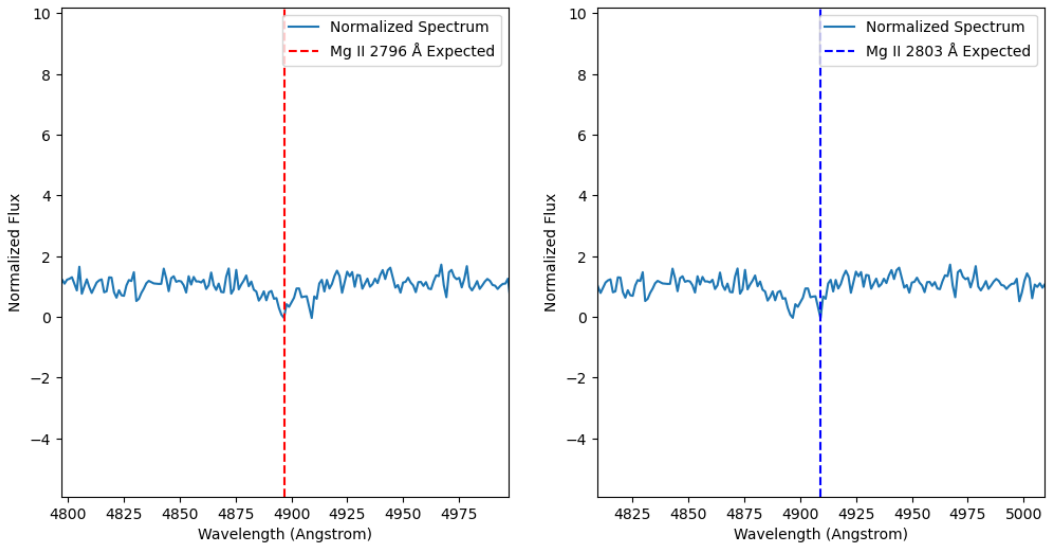

Figure 22: Example 1: Galaxy J124807.16+060111.8 showing clear Mg II $\lambda\lambda$2796, 2803 absorption features. However for this peculiar case the doublet was not blueshifted at all.

A.5 Code Availability

The full Python code used for spectral analysis, quasar querying, velocity calculation, and visualization is included as a separate file named `thesis_code.py`, attached alongside this thesis.

It uses publicly available libraries such as `astropy`, `specutils`, `matplotlib`, and `astroquery`, and is compatible with Python 3.8+.

Additionally, the code is also archived at: `https://github.com/harshsatasiya/poststarburst-mgii-thesis`